Hyperspherical approach to dipolar droplets beyond the mean-field limit

Eli J. Halperin and John L. Bohn
JILA, NIST, and Department of Physics, University of Colorado, Boulder, Colorado 80309-0440, USA

(Received 29 June 2021; accepted 26 August 2021; published 29 September 2021)

We apply a hyperspherical formulation to a trapped Bose-Einstein condensate with dipolar and contact interactions. Central to this approach is a general correspondence between K-harmonic hyperspherical methods and a suitable Gaussian ansatz to the Gross-Pitaevskii equation, regardless of the form of the interparticle potential. This correspondence allows one to obtain hyperspherical potential energies for a wide variety of physical problems. In the case of the dipolar Bose-Einstein condensate, this motivates the inclusion of a beyond-mean-field term within the hyperspherical picture, which allows us to describe the energies and wave functions of excitations of self-bound dipolar droplets outside the mean-field limit.

DOI: 10.1103/PhysRevA.104.033324

I. INTRODUCTION

Recently, a number of interesting phenomena have been observed in dipolar Bose-Einstein condensates (BECs), including dipolar droplets [1–4]. Dipolar droplets are self-bound collections of strongly dipolar atoms, where the droplets are elongated along the polarization axis. Here interatomic attraction is balanced by quantum fluctuations, leading to a metastable state which slowly evaporates due to three-body recombination. Dipolar droplets are considered self-bound as the droplet remains intact even after the trap is entirely removed.

Upon their discovery, it was immediately realized that these dipolar droplets could be described theoretically by an extended Gross-Pitaevskii equation (EGPE), the extension being the inclusion of fluctuation terms beyond the mean-field description [5]. The EGPE describes the self-binding and stability of the droplet [6,7], as well as its low-lying excitations [5,8].

In this paper we present an alternative theoretical approach to dipolar droplets, based on an explicit wave-function-based method. The method relies on choosing a small set of collective coordinates that represent the spatial extent of the full gas of atoms, rather than the coordinates of any one atom. By this means the basic properties of the gas are described, in the examples herein, by a two-dimensional *linear* Schrödinger equation. The usual intuitions of quantum mechanics can be applied, and explicit, albeit approximate, wave functions for excitations of the BEC can be shown. The method has similarities to the variational Gaussian ansatz approach for finding approximate ground-state solutions to the EGPE [6,7,9], as we will explore in detail. However, our method has the advantage that excited states of collective motion can be calculated as well.

The method recasts collective radial and axial coordinates of the atoms into their root-mean-square average coordinates, averaged over all atoms. These coordinates encompass the most basic properties of the BEC, namely, their overall size and collective excitations in radial and axial degrees of freedom. Mathematically, they represent hyperradii in a multidimensional configuration space, whereby the method is referred to as a hyperspherical approach.

Hyperspherical approaches to BECs have proven fruitful in the past, describing, for example, the stability of BECs with attractive contact potentials [10–12]; condensate fraction [13]; multicomponent BECs [14]; the influence of realistic two-body contact interactions, including effective range corrections [15–17] and even formally infinite scattering lengths [18–21]; realistic two-body interactions [22–24]; and condensate dynamics [25–27]. These treatments are all necessarily approximate, yet an exciting recent development shows that their accuracy can be enhanced by combining hyperspherical coordinates with solutions to the Gross-Pitaevskii equation (GPE) [28]. Further, hyperspherical methods can be fruitfully applied to fermionic gases as well [29–31].

This paper extends the hyperspherical approach to the case of a dipolar BEC. Instead of using a single hyperradius to describe the Bose gas, we use two hyperradii [32], describing the average displacement of the particles in the radial and axial directions. This allows us to effectively incorporate the dipole-dipole interaction into hyperspherical coordinates. In our approximation the two hyperradii are the only coordinates. We ignore the explicit dependence of the wave function on hyperangles, an approximation known as the K-harmonic approximation. This approach is therefore aimed at describing the ground state of the condensate, as well as collective excitations such as breathing and quadrupole modes, or variations of these.

Significantly, we show a general correspondence between all K-harmonic hyperspherical approaches and the Gaussian ansatz to the GPE regardless of the interparticle potential. We see that, in the limit of a large number of particles, the effective potential in the hyperspherical one-dimensional (1D) or 2D Schrödinger equation approaches the energy surface given by a suitable 1D or 2D Gaussian ansatz to the GPE. This insight vastly simplifies an entire class of hyperspherical

calculations when one is concerned with many-body physics. In the hyperspherical method, this energy surface plays the role of the potential energy, and thus we can compute excited states and condensate dynamics within the 2D Schrödinger equation, whereas the variational Gaussian ansatz is limited to ground states and low-lying excitations in a harmonic approximation. One can proceed alternatively by considering Bogoliubov excitations occurring on top of a variational ground state [33,34], a topic we will not pursue here.

Section II outlines the hyperspherical method with two hyperradii, showing the effective 2D Schrödinger equation. Section III shows the more general correspondence between the K-harmonic hyperspherical approximation and the Gaussian ansatz to the GPE. This allows us to translate the Lee-Huang-Yang (LHY) correction [35,36] into hyperspherical coordinates. We then apply this approach to the self-bound dipolar droplet in Sec. IV, showing excited states and spectra of the dipolar BEC.

II. HYPERSPHERICAL APPROACH

We consider a collection of N identical dipolar atoms of mass m in a cylindrically symmetric harmonic potential V_{ext} with radial trapping frequency ω_ρ and axial trapping frequency ω_z. The Hamiltonian is

$$H = \sum_{i=1}^{N}\left[-\frac{\hbar^2}{2m}\nabla_i^2 + V_{\text{ext}}(\mathbf{r}_i)\right] + \sum_{i<j}^{N}[V_{dd}(\mathbf{r}_{ij}) + V_c(\mathbf{r}_{ij})], \tag{1}$$

where V_{ext} is the external trapping potential and the dipole-dipole interaction V_{dd} pertains to a pair of dipoles polarized along the laboratory z axis

$$V_{dd}(\mathbf{r_{ij}}) = \frac{3\hbar^2}{m}\frac{a_{dd}}{r^3}(1 - 3\cos^2\theta). \tag{2}$$

Here the dipole length is defined as $a_{dd} \equiv m\mu_0\mu^2/12\pi\hbar^2$, with μ_0 the vacuum permeability and μ the atom's dipole moment, and θ is the angle between $\mathbf{r_{ij}}$ and the polarization axis. The two-body contact potential is given by

$$V_c(\mathbf{r_{ij}}) = \frac{4\pi\hbar^2 a}{m}\delta(\mathbf{r_{ij}}), \tag{3}$$

where a is the s-wave scattering length. Given that the dipole-dipole interaction and the trapping potential obey a cylindrical but not spherical symmetry (i.e., no φ dependence) and the other terms in the Hamiltonian have full spherical symmetry, we wish to describe a BEC in terms of its height in the z direction and its width in the x-y plane. To this end we introduce two collective hyperradii via

$$P^2 = \frac{1}{N}\sum_{i=1}^{N}\left(x_i^2 + y_i^2\right), \tag{4}$$

$$Z^2 = \frac{1}{N}\sum_{i=1}^{N} z_i^2. \tag{5}$$

Here P (understood as capital ρ) gives the root-mean-square displacement of the gas in the radial direction and Z the root-mean-square displacement in the axial direction. These two coordinates, along with $3N-2$ additional hyperangles, describe the complete configuration of the gas. In these coordinates, the external harmonic potential V_{ext} has a simple form

$$V_{\text{ext}} = \sum_{i}^{N}\left[\frac{1}{2}m\omega_\rho\rho_i^2 + \frac{1}{2}m\omega_z z_i^2\right] \tag{6}$$

$$= \frac{1}{2}M\omega_\rho P^2 + \frac{1}{2}M\omega_z Z^2, \tag{7}$$

where $M = mN$. The kinetic term T in Eq. (1) can now be written as [10,37]

$$T = -\frac{\hbar^2}{2M}\left[\frac{1}{P^{2N-1}}\frac{\partial}{\partial P}\left(P^{2N-1}\frac{\partial}{\partial P}\right) - \frac{\Lambda_P^2}{P^2}\right] - \frac{\hbar^2}{2M}\left[\frac{1}{Z^{N-1}}\frac{\partial}{\partial Z}\left(Z^{N-1}\frac{\partial}{\partial Z}\right) - \frac{\Lambda_Z^2}{Z^2}\right]. \tag{8}$$

Here Λ_P and Λ_Z are the two grand angular momentum operators, which behave in analogy with the 3D angular momentum operator. They are given by

$$\Lambda_P^2 = \sum_{i<j}\left[x_i\frac{\partial}{\partial x_j} - x_j\frac{\partial}{\partial x_i}\right]^2, \tag{9}$$

$$\Lambda_Z^2 = \sum_{i<j}\left[z_i\frac{\partial}{\partial z_j} - z_j\frac{\partial}{\partial z_i}\right]^2, \tag{10}$$

where in the first sum x_i is understood to be an element of the $2N$-dimensional vector $(x_1, y_1, x_2, y_2, \ldots, x_N, y_N)$. These operators obey the eigenvalue equations [37,38]

$$\Lambda_P Y_{\lambda\mu}^P = \lambda(\lambda + 2N - 2)Y_{\lambda\mu}^P, \tag{11}$$

$$\Lambda_Z Y_{\lambda\mu}^Z = \lambda(\lambda + N - 2)Y_{\lambda\mu}^Z. \tag{12}$$

Here μ stands for a degenerate set of indices for each eigenvalue λ that we will not specify here. These eigenvectors $Y_{\lambda\mu}^{(P,Z)}$ are the hyperspherical harmonics. In addition, $Y_{\lambda\mu}^P$ forms a complete orthonormal basis for $2N-1$ hyperangles and $Y_{\lambda\mu}^Z$ for $N-1$ hyperangles. It is implied that they are symmetric under exchange of identical bosons, although we need not perform this symmetrization explicitly for our purposes. We then expand an arbitrary many-body wave function ψ as

$$\psi = P^{(2N-1)/2}Z^{(N-1)/2}\sum_{\lambda\lambda'\mu\mu'} F_{\lambda\lambda'\mu\mu'}(P,Z)Y_{\lambda\mu}^P Y_{\lambda'\mu'}^Z. \tag{13}$$

The prefactor of $P^{(2N-1)/2}Z^{(N-1)/2}$ eliminates any first derivatives in $T\psi$. We end up with a new set of coupled Schrödinger

equations

$$\left(-\frac{\hbar^2}{2M}\left[\frac{\partial^2}{\partial P^2}+\frac{\partial^2}{\partial Z^2}-\frac{(2N-1)(2N-3)+4\lambda(\lambda+2N-2)}{4P^2}-\frac{(N-1)(N-3)+4\lambda'(\lambda'+N-2)}{4Z^2}\right]\right.$$
$$\left.+\frac{1}{2}M\omega_\rho P^2+\frac{1}{2}M\omega_z Z^2\right)F_{\lambda\lambda'\mu\mu'}+\sum_{\bar\lambda\bar\lambda'\bar\mu\bar\mu'}\left[\sum_{i<j}\langle\bar\lambda\bar\lambda'\bar\mu\bar\mu'|\,V_c(\mathbf{r_{ij}})+V_{dd}(\mathbf{r_{ij}})\,|\lambda\lambda'\mu\mu'\rangle\right]F_{\bar\lambda\bar\lambda'\bar\mu\bar\mu'}(P,Z)=EF_{\lambda\lambda'\mu\mu'}. \tag{14}$$

We expect that the general features of the condensate will emerge with a rather small expansion of states [10]. In fact, we choose the smallest possible expansion, known as the K-harmonic approximation, and thus set $\lambda=\lambda'=0$. We suppress the notation $\lambda\lambda'\mu\mu'$ in the following and denote the lowest hyperspherical harmonic as $|0\rangle$. We expect this should approximately represent the ground state and bulk dynamics of the condensate. Making this approximation, we have the simplified equation

$$\left(-\frac{\hbar^2}{2M}\left[\frac{\partial^2}{\partial P^2}+\frac{\partial^2}{\partial Z^2}-\frac{(2N-1)(2N-3)}{4P^2}-\frac{(N-1)(N-3)}{4Z^2}\right]+\frac{1}{2}M\omega_\rho^2P^2+\frac{1}{2}M\omega_Z^2Z^2\right.$$
$$\left.+\sum_{i<j}\langle 0|\,V_c(\mathbf{r_{ij}})+V_{dd}(\mathbf{r_{ij}})\,|0\rangle\right)F_0(P,Z)=EF_0(P,Z). \tag{15}$$

III. GENERAL RELATIONSHIP TO THE GROSS-PITAEVSKII EQUATION

We first consider the more general case where the two-body potential $V(\mathbf{r_{ij}})$ depends on the specific vector $\mathbf{r_{ij}}$ between two atoms. This will help us compute the specifics cases of V_c and V_{dd}. Selecting the single pair of particles $i=1$ and $j=2$, we define the hyperangles α and β such that

$$\rho_{12}=\sqrt{2N}P\sin\alpha, \tag{16}$$

$$z_{12}=\sqrt{2N}Z\sin\beta. \tag{17}$$

These hyperangles have associated hyperspherical surface area elements [37]

$$d\Omega^\alpha=\sin\alpha\cos^{2N-3}\alpha d\alpha, \tag{18}$$

$$d\Omega^\beta=\cos^{N-2}\beta d\beta. \tag{19}$$

Let ϕ give the angle for the unit vector $\hat\rho_{12}$. Then the total surface area over the entire hypersphere is

$$d\Omega^N d\Omega^{2N}=\sin\alpha\cos^{2N-3}\alpha\cos^{N-2}\beta d\alpha d\phi d\beta \times d\Omega^{N-1}d\Omega^{2N-2}. \tag{20}$$

The hyperspherical harmonics Y_0^P and Y_0^Z are constant across their respective hyperspheres. Since they are normalized, we have

$$Y_0^P=\sqrt{\frac{\Gamma(N)}{2\pi^N}}=\frac{1}{\sqrt{I(2N)}}, \tag{21}$$

$$Y_0^Z=\sqrt{\frac{\Gamma(N/2)}{2\pi^{N/2}}}=\frac{1}{\sqrt{I(N)}}, \tag{22}$$

where $I(k)$ stands for the hyperspherical surface area in k dimensions. Since these harmonics do no depend on hyperangles, each term in the sum in Eq. (15) is the same. Thus we have

$$V_{\rm int}=\sum_{i<j}\langle 0|\,V(\mathbf{r_{ij}})\,|0\rangle \tag{23}$$

$$=\frac{N(N-1)}{2}\langle 0|\,V(\mathbf{r_{12}})\,|0\rangle\,. \tag{24}$$

Using our definitions of the hyperangles, we have

$$V_{\rm int}=\frac{N(N-1)}{2}\frac{1}{I(2N)I(N)}\int V(\mathbf{r_{12}})\sin\alpha\cos^{2N-3}\alpha\cos^{N-2}\beta\,d\alpha\,d\phi\,d\beta\int d\Omega^{N-1}\int d\Omega^{2N-2} \tag{25}$$

$$=\frac{N(N-1)I(N-1)I(2N-2)}{2I(2N)I(N)(2N)^{3/2}P^2Z}\int V(\mathbf{r_{12}})\rho_{12}\left(1-\frac{z_{12}^2}{2NZ^2}\right)^{(N-3)/2}\left(1-\frac{\rho_{12}^2}{2NP^2}\right)^{N-2}d\rho_{12}dz_{12}d\phi \tag{26}$$

$$\approx\frac{N^2}{8\pi^{3/2}}\frac{1}{P^2Z}\int V(\mathbf{r_{12}})\exp\left(-\frac{z_{12}^2}{4Z^2}\right)\exp\left(-\frac{\rho_{12}^2}{2P^2}\right)\rho_{12}d\rho_{12}dz_{12}d\phi. \tag{27}$$

Equation (25) rephrases the angles in terms of interparticle coordinates according to Eqs. (16) and (17). In Eq. (27) we went to the large-N limit, using that

$$e^x=\lim_{n\to\infty}\left(1+\frac{x}{n}\right)^n \tag{28}$$

and that $N\approx N-2\approx N-3$. We also simplified the ratio of Γ functions present in the hyperspherical surface area elements. This expression is exact until the final line (27), where Gaussians emerge from the hyperangular volume elements.

Now we will compare this expression to the Gaussian ansatz to the GPE. The GPE, for purely contact interactions, is given by [39]

$$i\hbar\frac{\partial\phi}{\partial t}=\left[-\frac{\hbar^2}{2m}\frac{\partial^2}{\partial x^2}+V_{\rm ext}+g|\phi|^2\right]\phi. \tag{29}$$

Here $g = 4\pi\hbar^2 a/m$, with a the scattering length. One can find approximate ground states to Eq. (29) using a variational wave function and then minimizing the resulting energy functional. The 2D Gaussian ansatz to the GPE posits a variational wave function of the form

$$\phi = \left(\frac{N}{\pi^{3/2}\sigma_\rho^2\sigma_z}\right)^{1/2} \exp\left(\frac{\rho^2}{2\sigma_\rho^2}\right) \exp\left(\frac{z^2}{2\sigma_z^2}\right). \tag{30}$$

Here σ_ρ gives the width of the condensate in the radial direction and σ_z the width in the axial direction. This Gaussian ansatz wave function ϕ can be transformed to hyperspherical coordinates, giving the correspondence

$$Z = \frac{\sigma_z}{\sqrt{2}}, \tag{31}$$

$$P = \sigma_\rho. \tag{32}$$

In the variational ansatz to the GPE, the energy due to an arbitrary interaction is

$$E_{\rm int} = \frac{1}{2}\int d\mathbf{r_1} d\mathbf{r_2} |\phi_1|^2 |\phi_2|^2 V(\mathbf{r_{12}}). \tag{33}$$

Making a change of coordinates and computing this integral, we find that

$$E_{\rm int} = \frac{N^2}{4\sqrt{2}\pi^{3/2}} \frac{1}{\sigma_\rho^2\sigma_z} \int V(\mathbf{r_{12}}) \exp\left(-\frac{z_{12}^2}{2\sigma_z^2}\right) \times \exp\left(-\frac{\rho_{12}^2}{2\sigma_\rho^2}\right) \rho_{12} d\rho_{12} dz_{12} d\phi. \tag{34}$$

By using the correspondence given in Eqs. (31) and (32), Eq. (34) is seen to match Eq. (27), i.e., $V_{\rm int} = E_{\rm int}$. Other authors have noted the seeming similarity between these hyperspherical potentials $V_{\rm int}$ and energy functional of the Gaussian ansatz to the GPE (cf. Ref. [28]). We have shown that this resemblance is not simply coincidental; in the limit of a large number of particles they are in fact the same. The convergence in N is rapid for typical potentials; for $N = 10\,000$ particles and a δ-function interaction, the hyperspherical potential matches the Gaussian ansatz energy surface to within 0.03%. Additional terms in the Gaussian ansatz energy surface given by the external potential and the kinetic energy will match the external potential and centrifugal terms in the hyperspherical picture, respectively. In the 1D case, with a single hyperradius and a spherically symmetric Gaussian ansatz, the two approaches can also be shown to give the same potential energies in the large-N limit, following a similar argument as above. Philosophically similar simplifications in the large-N limit have been shown for a spherically symmetric Fermi gas [30,31]. In the case of dipolar BECs, the hyperspherical approach allows one to go beyond the Gaussian ansatz to the GPE, due to the kinetic energy terms in P and Z, which have no counterpart in the Gaussian ansatz approach. These terms allow us to compute excited states of the condensate and to extract a spectrum.

IV. DIPOLAR DROPLET

In order to adequately describe the dipolar droplet, it is necessary to incorporate the effects of fluctuations that go beyond the mean field [6,7]. We can exploit the close connection between our K-harmonic theory and the Gaussian ansatz to proceed as follows.

Within the Gaussian ansatz as in Eq. (30), fluctuations are accounted for via an additional term in the energy functional [6]

$$V_{\rm LHY} = c\frac{\hbar^2}{m}(Na)^{5/2} \frac{1 + \frac{3}{2}\frac{a_{dd}^2}{a^2}}{\sigma_\rho^3\sigma_z^{3/2}}, \tag{35}$$

where $c = 2^{19/2}/75\sqrt{5}\pi^{7/4} \approx 0.35$. The correspondence between the hyperspherical picture and the Gaussian ansatz to the GPE motivates the inclusion of an LHY hyperspherical potential. The Gaussian widths set the hyperradii as in Eqs. (31) and (32). We thus have

$$V_{\rm LHY} = \frac{c}{2^{3/4}}\frac{\hbar^2}{m}(Na)^{5/2} \frac{1 + \frac{3}{2}\frac{a_{dd}^2}{a^2}}{P^3 Z^{3/2}}. \tag{36}$$

This potential should be a good approximation in the large-N limit relevant to experiments, although is still not formally justified then. Deriving such a correction from first principles in the hyperspherical formalism remains an outstanding question. In this limit, the rest of the hyperspherical potential surface simplifies, and we are left with

$$\Bigg[-\frac{\hbar^2}{2M}\left(\frac{\partial^2}{\partial P^2} + \frac{\partial^2}{\partial Z^2}\right) + \underbrace{\frac{\hbar^2}{2M}\frac{N^2}{P^2} + \frac{\hbar^2}{2M}\frac{N^2}{4Z^2} + \frac{1}{2}M\omega_\rho^2 P^2 + \frac{1}{2}M\omega_z^2 Z^2 + V_c + V_{dd} + V_{\rm LHY}}_{V_{\rm eff}}\Bigg] F_0 = E F_0. \tag{37}$$

Using the large-N limit of the interaction terms in $V_{\rm eff}$, we find (see the Appendix)

$$V_c(P, Z) = \frac{\hbar^2 a}{2m\sqrt{\pi}} \frac{N^2}{ZP^2} \tag{38}$$

for the contact term, where a is the scattering length, and

$$V_{dd} = \frac{\hbar^2 a_{dd} N^2}{4m\sqrt{\pi}} \frac{1}{ZP^2}\left[4 + \frac{12}{\lambda^2 - 2} - \frac{6\sqrt{2}\lambda^2}{(\lambda^2 - 2)^{3/2}} \cot^{-1}\left(\sqrt{\frac{2}{\lambda^2 - 2}}\right)\right] \tag{39}$$

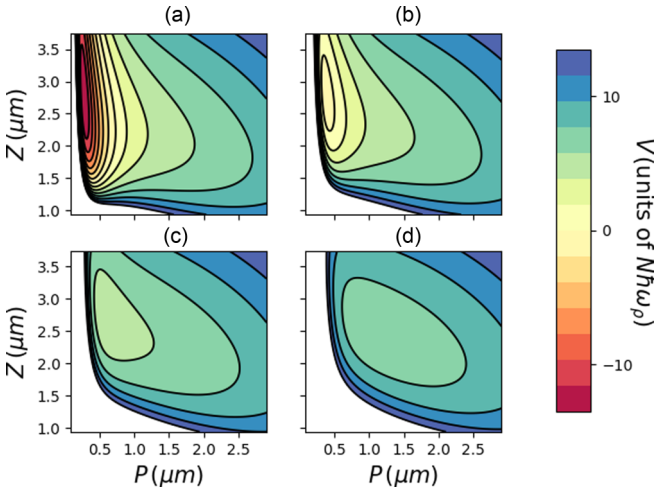

FIG. 1. Potential surfaces V_{eff} for 2×10^4 ^{164}Dy atoms in a $70 \times 2\pi$ Hz spherical trap. The scattering length a takes values (a) $70a_0$, (b) $80a_0$, (c) $90a_0$, and (d) $100a_0$. The droplet, given by the minimum on the far left plots in (a) and (b), is present for $a = 70a_0$ and $80a_0$, but not for $a = 90a_0$ or $100a_0$.

for the dipole term. Here $\lambda = P/Z$. Although these could have been determined from the correspondence to the energy functional in the Gaussian ansatz to the GPE, the Appendix gives a derivation of these terms within the hyperspherical formalism before then taking the large-N limit.

V. DROPLET TO GAS TRANSITION IN A SPHERICAL TRAP

We now apply the hyperspherical method to a collection of dipolar dysprosium atoms held in a spherical trap. We consider system parameters similar to Refs. [8,9] where, as the scattering length is increased, the ground state evolves smoothly from a self-bound droplet to a gaseous dipolar BEC held together by the trap potential. In this case the ground state and collective excitation spectrum were explored within the Gaussian ansatz [9] and by calculating the Bogoliubov excitation spectrum [8]. Our emphasis here will be on presenting these spectra in terms of the wave functions in our linear two-dimensional Schrödinger equation and especially how these wave functions evolve across the transition.

A. Potential energy surface

We consider a BEC with $N = 2 \times 10^4$ ^{164}Dy atoms in a harmonic trap with $\omega_\rho = \omega_z = 70 \times 2\pi$ Hz. The atoms are aligned along the z axis and have dipole length $a_{dd} = 131a_0$. Figure 1 shows the resulting hyperspherical potential surface at four different scattering lengths in a spherically symmetric trap.

For $a = 70a_0$ [Fig. 1(a)] the minimum corresponds to a droplet state that is deeply bound at $P = 0.28$ μm and $Z = 2.73$ μm. This minimum is present without the trapping potential, and thus the state located here is a self-bound droplet. Because $Z > P$, the physical density profile of the droplet is elongated along the z axis. At $a = 80a_0$ [Fig. 1(b)], the droplet is less deeply bound, although this minimum would still exist in the absence of the trap. Here the droplet is somewhat wider, with $P = 0.39$ μm while $Z = 2.75$ μm, a significant change from $a = 70a_0$ in the width of the condensate while the height is nearly constant.

Note that for all the potential surfaces shown, there is only one local minimum. This is not the case in different trap geometries, which are squeezed more tightly in z than in ρ. In these pancake traps, there are two local minima which may coexist, corresponding to the pancake-shaped gas and the droplet. As the scattering length changes in this scenario, the global condensate ground state abruptly changes from the droplet to the gas as one increases a.

B. Spectrum across the transition

These potential energy surfaces correspond to the energy functional as generated by the Gaussian variational ansatz to the Gross-Pitaevskii equation. If that functional is treated *as if* it were a potential energy surface [9], it can be used to assess the character of the low-lying modes by examining harmonic expansions of the functional around its minima. By contrast, the hyperspherical approach explicitly shows the role of this potential surface and thus can generate excited-state spectra and wave functions directly from our effective 2D Schrödinger equation (37) without using any harmonic approximations.

A portion of the spectrum is shown as a function of scattering length in the center panel of Fig. 2 (black solid lines). The Bogoliubov spectrum in Fig. 3 of Ref. [8] shares the essential feature of our figure, namely, the softening of the excited-state energies as the scattering length passes from low to high. Note that Fig. 3 of Ref. [8] contains all angular momentum projections $m = 0, 1, \ldots 5$, whereas Fig. 2 of the present paper corresponds only to states with $m = 0$, as considering two hyperradii in the K-harmonic approximation maintains cylindrical symmetry for all modes.

For comparison, the first two such $m = 0$ excited-state energies, as computed in the Bogoliubov approximation, are shown (blue dashed lines), reproduced from Ref. [8]. For the first excited state, the K-harmonic approximation agrees extremely well with the Bogoliubov energy, while for the second excited state the two display only qualitative agreement. Other hyperspherical methods show similar behavior [10], where the first hyperspherical excited-state energy closely agrees with the first Bogoliubov excited-state energy, while the energies of higher excited states disagree.

We now focus on the properties of excited states in the K-harmonic approximation. For scattering lengths $a < 90a_0$, the spectrum consists of two sets of relatively evenly spaced levels, with very different spacings between the two sets. At $a = 90a_0$, the lower-energy set of levels, with spacing 158 Hz, belongs to excitations along the Z axis, as is verified by the sample wave functions plotted to the left of the main figure. The higher energies, with characteristic spacings 1213 Hz, correspond to excitations in the P coordinate. Even here, a harmonic approximation gives this higher excitation energy instead as 1225 Hz, a 1% discrepancy. The potential energy surface is nearly separable in these coordinates, as might be expected from the potentials shown in Fig. 1. These excitations in P rapidly decline in energy as a grows, since the

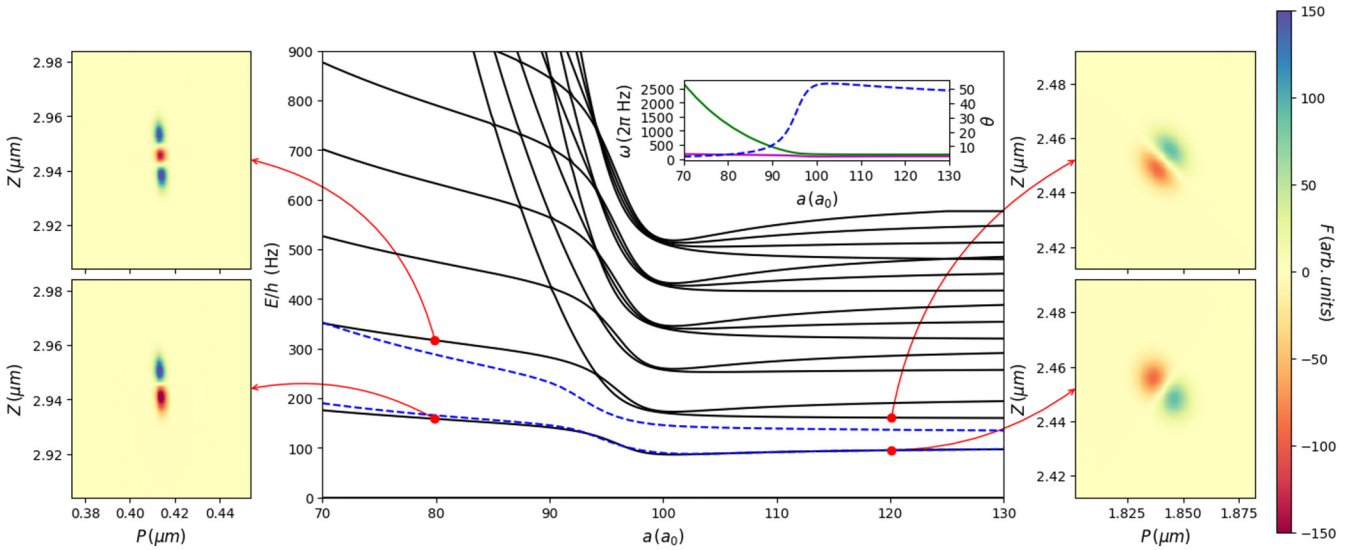

FIG. 2. Spectrum of excited states relative to the ground-state energy as a function of the scattering length, shown by black solid lines. Here $N = 2 \times 10^4$ and $a_{dd} = 131a_0$. The left portion of the plot shows excitations of the dipolar droplet, while the right portion shows excitations of the trapped gas. A smooth transition occurs between these two regimes as the modes soften. The first two excited states are shown for two characteristic scattering length of $80a_0$ and $120a_0$, on left when the BEC is in the droplet phase and on right when the BEC is in the gaseous phase. Blue dashed lines show the spectrum obtained by a Bogoliubov method (reproduced from Ref. [8] with permission). Note the different axes in the far left and far right columns, while the scale remains constant

outward pressure of a larger scattering length acts to broaden the gas in the radial direction, as also seen in Fig. 1.

As the scattering length increases beyond around $90a_0$, the energy levels coalesce into bands with levels nearly degenerate in each band. For $a > 100a_0$, the levels become more evenly spaced and depend only weakly on scattering length. In this regime, the BEC is well described by a mean-field picture, i.e., quantum fluctuations are not required for stability. Here the spectrum resembles that of a 2D harmonic oscillator with primary excitation frequencies $E/h = 95$ and 161 Hz. In this case, the energy levels nearly exactly match what one would expect from the effective harmonic excitation frequencies of the hyperspherical potential for all energies shown.

The right column of Fig. 2 shows wave functions for the first two excited states of the system at $a = 120a_0$. Here, in the gaseous state of the dipolar BEC, the symmetry of the wave functions has changed. The lowest excitation has a nodal line running from lower left to upper right. This corresponds to an excitation where as P gets large, Z gets small, and vice versa: a quadrupole mode. In the next excited state, the nodal line runs from upper left to lower right. In this excitation both P and Z grow and shrink in phase, as in a breathing mode.

We can characterize normal modes of the hyperspherical potential near its minimum. This is similar in spirit to the modes generated by the Gaussian ansatz method [9] but of course in our picture corresponds to the physical modes of an actual potential surface. The inset of Fig. 2 shows these two effective frequencies (solid lines) plotted on the left-hand axis.

The normal modes of the hyperspherical potential surface describe oscillations in the P-Z plane that occur along tilt angles that are roughly $\theta = 0$ and $\theta = \pi/2$ relative to the Z axis. For a surface whose expansion near its minimum is given by

$$V(P, Z) = AP^2 + BZ^2 + CPZ, \tag{40}$$

with $A, B, C > 0$, the tilt angle is given by

$$\theta = \tan^{-1}\left(\frac{C(B-A)}{(A-B)^2 + \sqrt{(A-B)^4 + (A-B)^2C^2}}\right) \tag{41}$$

for $A \neq B$. When $A = B$ the tilt angle is not well defined. In the inset to Fig. 2, this tilt angle is shown as a blue dashed line using the right-hand axis. The tilt evolves from $\theta = 4.2^\circ$ for $a = 80a_0$ to $\theta = 50.4^\circ$ for $a = 120a_0$, thus quantifying the rotation from either P or Z dominated modes in the droplet to breathing and quadrupole modes in the gaseous state.

C. Evolution of eigenstates

In both of these regimes, where the dipolar BEC is clearly in one of the gaseous or droplet phases, analysis of the energy surface [9] elucidates the essential properties described by the hyperspherical approach. However, in the intermediate regime, where excitation frequencies are seen to fall sharply as a increases and the system transitions from the droplet to the gas, such harmonic approximations begin to fail. In this region, the energy levels are seen to form into bands. In each band, as a gets smaller than $90a_0$, all but one excitation, corresponding to states with at least one quantum in the radial direction, increase rapidly. Here a single energy level peels off and forms the Z-excitation spectrum of the droplet.

The evolution of the character of these states across the transition is best illustrated by states that are somewhat excited above the ground state. Accordingly, Fig. 3 shows a zoomed-in spectrum in this critical regime as well as states from one such band of excited states, namely, the $n = 12$–15 states at four different values of a in this regime. The top panel of Fig. 3 shows this spectrum for the first 19 excited states. The energy levels are grouped into bands of an increasing number of states, with $\lfloor n/2 + 1 \rfloor$ states in the nth band. These

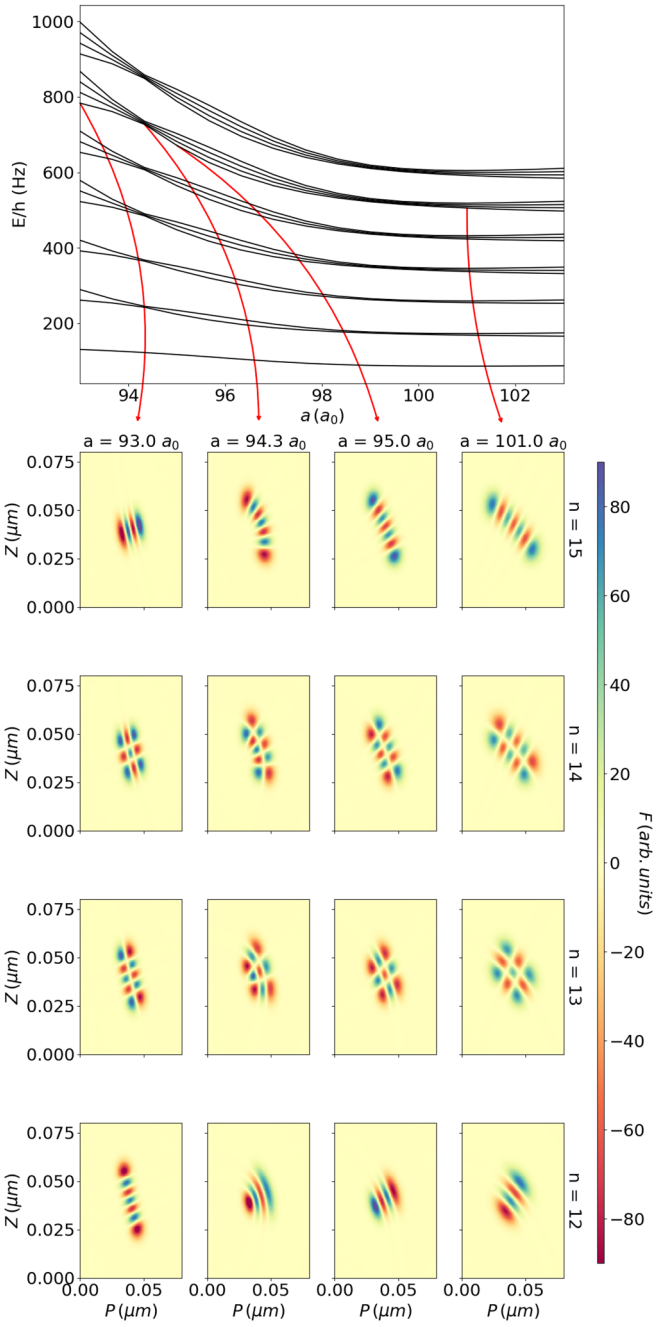

FIG. 3. Spectrum and excited states while the dipolar BEC transitions between the droplet and gaseous phases, with the spectrum shown in the top panels and corresponding excited state in the spectrum shown below. Red arrows indicate which excited states are shown. The excited states are not described by harmonic oscillator states, exhibiting curved and distorted profiles as the BEC transitions from the droplet to gaseous phase.

bands all exhibit a crossing occurring at roughly the same value of a, namely, $a \approx 94.3a_0$. All the given energy levels in a band are nearly degenerate at this point. Furthermore, the energy levels again become nearly degenerate around $a = 100a_0$. The red arrows in the sixth energy band indicate the energies levels shown below.

The bottom portion of Fig. 3 shows the excited states with $n = 15$, 14, 13, and 12, as labeled, corresponding to the red arrows in the above spectrum. Each of these states is shown at four different values of a, with the first, second, third, and fourth columns showing the states at $a = 93a_0$, $94.3a_0$, $95a_0$, and $101a_0$, respectively. For simplicity, the x and y axes both start at 0, so the position of the excited states in the P-Z plane is not shown. This way of plotting emphasizes comparing the shapes of the excited states, without regard to how they follow the minimum of the hyperspherical potential.

In the droplet (left column, $a = 93a_0$), the states follow the general pattern established above. The $n = 12$ state represents an excitation principally along the elongated z axis of the droplet, while $n = 15$, higher in energy, is principally a radial excitation. Note that there is already a degree of tilt in these patterns, indicating that the hyperspherical potential energy surface is not quite separable in the P and Z coordinates for excited states, but only approximately so. The intermediate states with $n = 13, 14$ contain quanta in both the P and Z directions.

Past the regions of avoided crossings and into the gaseous regime, the states at $a = 101a_0$ (right-hand column) have a different character. Here the $n = 12$ state, lowest in energy, has a nodal pattern describing a breathing mode of the gas. The higher-lying $n = 15$ state shows the excitation pattern of a quadrupole. Again, the intermediate states reveal quanta in both modes.

In the transition regime this is no longer the case. Consider the value $a = 94.3a_0$ (second column), corresponding to the first energy level crossing seen in the transition region, where the four given states are nearly degenerate, although not exactly so. The $n = 15$ state (second column, first row) exhibits a clearly curved character. Here the state is clearly not decomposable into two harmonic states about any two straight axes. The second state shown in this column, the $n = 14$ state, looks similar, with another excitation in the direction orthogonal to the curvature of the wave function. The state at $n = 13$ has one more such quantum, while $n = 12$ possesses only excitations in this other direction. This nonseparable behavior is the way the BEC negotiates its transition between the modes of the droplet and those of the gas. Even somewhat away from the degeneracy, at $a = 95a_0$, the excited states nonetheless exhibit a curved character.

We can additionally track the states at the same excitation number between the first and second columns. Following the level crossing, the states at the same excitation number look completely different than before. However, the $n = 15$ state at $a = 93a_0$ (first column, first row) state closely resembles the $n = 12$ at $a = 94.3a_0$ (second column, fourth row), with some distortion, and likewise for the $n = 12$ state at $a = 93a_0$ (first column, fourth row) and the $n = 15$ state at $a = 94.3a_0$ (second column, first row). These two states swap spectral positions while tracking continuously changing wave functions. The same effect can be seen looking at states $n = 13$ and 14 moving between $a = 93a_0$ and $94.3a_0$, where these two states swap places. The final two columns show the states before and after their second avoided crossing in the spectrum in this range of scattering length. However, here the state at a given excitation number looks much the same on either side of the crossing. As one goes to larger scattering lengths, the curved nature of these states begins to disappear. The states once

again become well described by harmonic oscillator modes in two tilted directions.

VI. CONCLUSION

We applied a hyperspherical approach to a dipolar quantum gas. In order to describe dipolar droplets, we first demonstrated a general correspondence between the hyperspherical approach and the Gaussian ansatz to the GPE. This allowed us to translate the LHY correction to our 2D Schrödinger equation, which removes the nonlinearity from the description of dipolar BEC. We showed excited-state energies and wave functions of the dipolar droplet. Especially in the phase transition regime, one must take into account the full potential where it is not well approximated by a harmonic oscillator in both directions.

The hyperspherical approach thus presents an intriguing middle ground between the full Bogoliubov excited spectrum and the intuitive Gaussian variational ansatz method. The hyperspherical approach preserves the appealing intuition of the latter, but affords its extension to higher excited collective modes that lie beyond a simple expression as separable modes in an effective harmonic oscillator. Further extensions of the approach could account for the tunneling of barely bound droplets into the gaseous state, much as the macroscopic tunneling of BECs with attractive interactions was studied [10]. Additionally, the hyperspherical approach could be employed to follow the dynamics of dipolar gases via the usual expansion of a linear system into energy eigenstates, providing an alternative view of the numerical evolution of the nonlinear EGPE.

ACKNOWLEDGMENTS

The authors thank D. Baillie and P. B. Blakie for generously sharing their Bogoliubov data, as well as the anonymous referees for suggesting this comparison. This material is based upon work supported by the National Science Foundation under Grant No. PHY 1734006.

APPENDIX: DIRECT CALCULATION OF HYPERSPHERICAL INTEGRALS

Here we obtain expressions for the hyperspherical potential surface for arbitrary N. We compute the effective potentials for both contact and dipolar interactions and then verify that these do indeed reduce to simpler forms that match the Gaussian ansatz to the GPE in the large-N limit. For a two-body contact potential of the form

$$V_c(\mathbf{r_{ij}}) = \frac{4\pi\hbar^2 a}{m}\delta(\mathbf{r_{ij}}), \tag{A1}$$

we need to find

$$V_c(P,Z) = \sum_{i<j}\int d\Omega\, Y_{00}^*(\Omega) V_c(\mathbf{r}_{ij}) Y_{00}(\Omega) \tag{A2}$$

$$= \frac{N(N-1)}{2}\int d\Omega\, Y_{00}^*(\Omega) V_c(\mathbf{r}_{12}) Y_{00}(\Omega). \tag{A3}$$

Note that $V_c(P,Z)$ refers to the effective hyperspherical potential while $V_c(\mathbf{r_{ij}})$ refers to the actual two-body potential. We can evaluate this directly, as the δ function vastly simplifies Eq. (26). We find that

$$V_c = \frac{\hbar^2 a(N-1)}{\sqrt{2\pi N}m}\frac{1}{ZP^2}\frac{\Gamma(\frac{N}{2})(N-1)}{\Gamma\left(\frac{N}{2}-\frac{1}{2}\right)} \tag{A4}$$

$$\approx \frac{\hbar^2 a}{2m\sqrt{\pi}}\frac{N^2}{ZP^2}. \tag{A5}$$

Here Eq. (A5) was obtained by using the large-N limit of the Γ functions. This approximate expression matches the term obtained in the Gaussian ansatz to the GPE [6].

For the dipolar potential, we have

$$V_{dd}(\mathbf{r}) = \frac{3\hbar^2}{m}\frac{a_{dd}}{r^3}(1-3\cos^2\theta). \tag{A6}$$

Here the dipole length is defined as $a_{dd} \equiv m\mu_0\mu^2/12\pi\hbar^2$ and θ is the angle between the $\mathbf{r}$ and the polarization axis. We can find a 1D integral expression for $V_{dd}(P,Z)$, which simplifies in the large-N limit.

We work in momentum space because it will later allow us to deal with the $1/r^3$ singularity in the dipole-dipole potential. We define the unit vectors [38]

$$\hat{u}_P = \frac{1}{P\sqrt{N}}(x_1, y_1, x_2, y_2, \ldots, x_N, y_N), \tag{A7}$$

$$\hat{u}_Z = \frac{1}{Z\sqrt{N}}(z_1, z_2, \ldots, z_N), \tag{A8}$$

$$\hat{w}_P = \frac{1}{\sqrt{2}k|\sin\theta_k|}(k_x, k_y, -k_x, -k_y, 0, \ldots, 0), \tag{A9}$$

$$\hat{w}_Z = \frac{1}{\sqrt{2}k|\cos\theta_k|}(k_z, -k_z, 0, \ldots, 0), \tag{A10}$$

with k and θ_k having the usual definitions for writing (k_x, k_y, k_z) in spherical polar coordinates. Notice that $\hat{u}$ depends only on position coordinates and $\hat{w}$ depends only on momentum coordinates. Using these unit vectors, we can embed the plane wave in the larger hyperspheres [38]

$$e^{i\vec{k}\cdot\vec{r}_{12}} = e^{i\sqrt{2N}kP|\sin\theta_k|\hat{w}_P\cdot\hat{u}_P} e^{i\sqrt{2N}kZ|\cos\theta_k|\hat{w}_Z\cdot\hat{u}_Z} \tag{A11}$$

$$= \frac{(2N-2)!!(N-2)!!}{Y_{00}^2}\sum_{\lambda_P,\mu_P} i^{\lambda_P} j_{\lambda_P}^{2N}(\sqrt{2N}kP|\sin\theta_k|) \times Y_{\lambda_P\mu_P}^*(\hat{w}_P) Y_{\lambda_P\mu_P}(\hat{u}_P) \sum_{\lambda_Z,\mu_Z} i^{\lambda_Z} j_{\lambda_Z}^N \times (\sqrt{2N}kZ|\cos\theta_k|) Y_{\lambda_Z\mu_Z}^*(\hat{w}_Z) Y_{\lambda_Z\mu_Z}(\hat{u}_Z). \tag{A12}$$

We embedded the first term in the $2N$-dimensional P space and the second term in the N-dimensional Z space. Here j^d are the hyperspherical Bessel functions in d dimensions. We also use the three-dimensional Fourier transform of $V_{dd}(\vec{r}_{12})$, $\widetilde{V_{dd}}(\vec{k}) = \frac{\hbar^2 a_{dd}}{m}\sqrt{\frac{2}{\pi}}(3\cos^2\theta_k - 1)$. Now

$$V_{dd}(P,Z) = \frac{N(N-1)}{2}\int d\Omega\, Y_{00} V(\vec{r}_{12}) Y_{00}$$

$$= \frac{N(N-1)}{2}\frac{\hbar^2 a_{dd}}{2\pi^2 m}(2N-2)!!(N-2)!! \times \int d^3\vec{k}(3\cos^2\theta_k - 1) j_0^{2N}(\alpha k) j_0^N(\beta k). \tag{A13}$$

Here $\alpha = \sqrt{2N}P|\sin\theta_k|$ and $\beta = \sqrt{2N}Z|\cos\theta_k|$. The hyperspherical Bessel functions can be written in terms of the standard spherical Bessel functions, giving

$$V_{dd}(P,Z) = N(N-1)\frac{\hbar^2 a_{dd}}{\pi^2 m}\Gamma(N)\Gamma\left(\frac{N}{2}\right)2^{3N/2-4} \times \underbrace{\int d^3\vec{k}(3\cos^2\theta_k - 1)\frac{J_{N-1}(\alpha k)J_{N/2-1}(\beta k)}{(\alpha k)^{N-1}(\beta k)^{N/2-1}}}_{I}. \tag{A14}$$

Then

$$I = \int d\hat{k}\frac{3\cos^2\theta_k - 1}{\alpha^{N-1}\beta^{N/2-1}}\underbrace{\int_0^\infty k^2 dk\frac{J_{N-1}(\alpha k)J_{N/2-1}(\beta k)}{k^{3N/2-2}}}_{I_k}.$$

The integral I_k needs to be broken up into two cases to be done analytically: one when $\alpha > \beta$ and one when $\alpha < \beta$. Since the integrand does not diverge when $\alpha = \beta$, we can safely split the integral into two components. Using [40], we get

$$I_k = \frac{\Gamma(\frac{3}{2})}{2^{3N/2-4}} \times \begin{cases} \frac{\alpha^{N-1}\beta^{N/2-4}}{\Gamma((N-3)/2)\Gamma(N)}F\left(\frac{3}{2}, \frac{5-N}{2}; N; x^2\right), & x > 1 \\ \frac{\alpha^{N-4}\beta^{N/2-1}}{\Gamma((2N-3)/2)\Gamma(N/2)}F\left(\frac{3}{2}, \frac{5-2N}{2}; \frac{N}{2}; y^2\right), & y > 1. \end{cases} \tag{A15}$$

Here we have defined $x \equiv \alpha/\beta$ and $y \equiv 1/x$, while F denotes the ordinary (Gaussian) hypergeometric functions. In order to proceed further here, we turn to the large-N limit of these hypergeometric functions. From the definitions of these functions we can write

$$\begin{aligned} F\left(\frac{3}{2}, \frac{5-N}{2}; N; x^2\right) &= \sum_{k=0}^{\infty}\frac{\left(\frac{3}{2}\right)_k\left(\frac{5-N}{2}\right)_k}{(N)_k}\frac{x^{2k}}{k!} \\ &\approx \sum_{k=0}^{\infty}\left(\frac{3}{2}\right)_k\frac{\left(-\frac{x^2}{2}\right)^k}{k!} \\ &\approx (1+x^2)^{-3/2}. \end{aligned}$$

Here $(z)_k$ gives the rising factorial. Between the first and second lines we have simplified ratios to their limiting values in the large-N limit. This sum then matches the Taylor expansion of the function given in the third line. Likewise,

$$F\left(\frac{3}{2}, \frac{5-2N}{2}; \frac{N}{2}; y^2\right) \approx (1+2y^2)^{-3/2}.$$

Since there is cylindrical symmetry, as well as mirror symmetry through the x-y plane, we can then rewrite the angular integral as

$$I = 4\pi\int_0^{\pi/2}\sin\theta_k d\theta_k\frac{3\cos^2\theta_k - 1}{\alpha^{N-1}\beta^{N/2-1}}I_k.$$

Now define $\theta_= \equiv \cot Z/P$. Note that $0 \leqslant \theta_= \leqslant \pi/2$, and at $\theta_=$ we have $\alpha = \beta$. For $0 \leqslant \theta < \theta_=$ we see that $\alpha < \beta$ and for $\pi/2 \geqslant \theta > \theta_=$ we see that $\beta > \alpha$. This will let us use our two cases for I_k,

$$\begin{aligned} I &= 4\pi\int_0^{\theta_=}\sin\theta_k d\theta_k\frac{3\cos^2\theta_k - 1}{\alpha^{N-1}\beta^{N/2-1}}I_k \\ &\quad + 4\pi\int_{\theta_=}^{\pi/2}\sin\theta_k d\theta_k\frac{3\cos^2\theta_k - 1}{\alpha^{N-1}\beta^{N/2-1}}I_k \end{aligned} \tag{A16}$$

$$\begin{aligned} &\approx \frac{4\pi\Gamma(\frac{3}{2})}{2^{3N/2-4}(2N)^{3/2}}\frac{1}{ZP^2}\Bigg[\frac{1}{\Gamma((N-3)/2)\Gamma(N)} \\ &\quad \times\int_0^1 dx\frac{x(2P^2 - Z^2x^2)}{P^2 + Z^2x^2}\left(\frac{1+x^2}{2}\right)^{-3/2} \\ &\quad + \frac{1}{\Gamma((2N-3)/2)\Gamma\left(\frac{N}{2}\right)}\int_0^1 dy\frac{2P^2y^2 - Z^2}{P^2y^2 + Z^2}(1+2y^2)^{-3/2}\Bigg], \end{aligned} \tag{A17}$$

where we used our definitions for x and y and then plugged in the asymptotic form of the hypergeometric functions. Finally, x and y have become dummy variables in the integral, and we can join these into a single integral in x. These equations will be useful in calculating the contact potential. So we can now write down V_{dd} in the large-N limit as

$$\begin{aligned} V_{dd} \approx \frac{\hbar^2 a_{dd}N^2}{4m\sqrt{\pi}}\frac{1}{ZP^2}\Bigg[&\int_0^1 dx\frac{x(2P^2 - Z^2x^2)}{P^2 + Z^2x^2}\left(1 + \frac{x^2}{2}\right)^{-3/2} \\ &+ 2\sqrt{2}\int_0^1 dy\frac{2P^2y^2 - Z^2}{P^2y^2 + Z^2}(1+2y^2)^{-3/2}\Bigg], \end{aligned} \tag{A18}$$

where we use the limiting form of the ratios of Γ functions, which converge quite rapidly. These integrals have a closed-form expression, when we express this in terms of the aspect ratio $\lambda = P/Z$. Using [40], we arrive at

$$\begin{aligned} V_{dd} \approx \frac{\hbar^2 a_{dd}N^2}{4m\sqrt{\pi}}\frac{1}{ZP^2}\Bigg[&4 + \frac{12}{\lambda^2 - 2} \\ &- \frac{6\sqrt{2}\lambda^2}{(\lambda^2-2)^{3/2}}\cot^{-1}\left(\sqrt{\frac{2}{\lambda^2-2}}\right)\Bigg]. \end{aligned} \tag{A19}$$

Note that there is no issue with divergence at $\lambda = \sqrt{2}$, as the diverging terms of this expression cancel there. This matches the large-N limit of the relevant term in the Gaussian ansatz to the GPE [6].

[1] I. Ferrier-Barbut, H. Kadau, M. Schmitt, M. Wenzel, and T. Pfau, Observation of Quantum Droplets in a Strongly Dipolar Bose Gas, Phys. Rev. Lett. **116**, 215301 (2016).

[2] H. Kadau, M. Schmitt, M. Wenzel, C. Wink, T. Maier, I. Ferrier-Barbut, and T. Pfau, Observing the Rosensweig instability of a quantum ferrofluid, Nature (London) **530**, 194 (2016).

[3] L. Chomaz, S. Baier, D. Petter, M. J. Mark, F. Wächtler, L. Santos, and F. Ferlaino, Quantum-Fluctuation-Driven Crossover from a Dilute Bose-Einstein Condensate to a Macrodroplet in a Dipolar Quantum Fluid, Phys. Rev. X **6**, 041039 (2016).

[4] M. Schmitt, M. Wenzel, F. Böttcher, I. Ferrier-Barbut, and T. Pfau, Self-bound droplets of a dilute magnetic quantum liquid, Nature (London) **539**, 259 (2016).
[5] A. R. P. Lima and A. Pelster, Quantum fluctuations in dipolar Bose gases, Phys. Rev. A **84**, 041604(R) (2011).
[6] D. Baillie, R. M. Wilson, R. N. Bisset, and P. B. Blakie, Self-bound dipolar droplet: A localized matter wave in free space, Phys. Rev. A **94**, 021602(R) (2016).
[7] R. N. Bisset, R. M. Wilson, D. Baillie, and P. B. Blakie, Ground-state phase diagram of a dipolar condensate with quantum fluctuations, Phys. Rev. A **94**, 033619 (2016).
[8] D. Baillie, R. M. Wilson, and P. B. Blakie, Collective Excitations of Self-Bound Droplets of a Dipolar Quantum Fluid, Phys. Rev. Lett. **119**, 255302 (2017).
[9] F. Wächtler and L. Santos, Ground-state properties and elementary excitations of quantum droplets in dipolar Bose-Einstein condensates, Phys. Rev. A **94**, 043618 (2016).
[10] J. L. Bohn, B. D. Esry, and C. H. Greene, Effective potentials for dilute Bose-Einstein condensates, Phys. Rev. A **58**, 584 (1998).
[11] D. K. Watson and B. A. McKinney, Improved large-N limit for Bose-Einstein condensates from perturbation theory, Phys. Rev. A **59**, 4091 (1999).
[12] A. Biswas, T. K. Das, L. Salasnich, and B. Chakrabarti, Stability of an attractive bosonic cloud with van der Waals interaction, Phys. Rev. A **82**, 043607 (2010).
[13] S. K. Haldar, B. Chakrabarti, S. Bhattacharyya, and T. K. Das, Condensate fraction and critical temperature of interacting Bose gas in anharmonic trap, Eur. Phys. J. D **68**, 262 (2014).
[14] T. Sogo, O. Sørensen, A. S. Jensen, and D. V. Fedorov, Stability and structure of two coupled boson systems in an external field, Phys. Rev. A **69**, 062504 (2004).
[15] O. Sørensen, D. V. Fedorov, and A. S. Jensen, Two-body correlations in N-body boson systems, Phys. Rev. A **66**, 032507 (2002).
[16] O. Sørensen, D. V. Fedorov, and A. S. Jensen, Correlated N-boson systems for arbitrary scattering length, Phys. Rev. A **68**, 063618 (2003).
[17] O. Sørensen, D. V. Fedorov, and A. S. Jensen, Structure of boson systems beyond the mean field, J. Phys. B **37**, 93 (2003).
[18] M. Thøgersen, D. V. Fedorov, and A. S. Jensen, Trapped Bose gases with large positive scattering length, Europhys. Lett. **79**, 40002 (2007).
[19] M. L. Lekala, B. Chakrabarti, G. J. Rampho, T. K. Das, S. A. Sofianos, and R. M. Adam, Behavior of trapped ultracold dilute Bose gases at large scattering length near a Feshbach resonance, Phys. Rev. A **89**, 023624 (2014).
[20] Y. Ding and C. H. Greene, Renormalized contact interaction in degenerate unitary Bose gases, Phys. Rev. A **95**, 053602 (2017).
[21] M. W. C. Sze, A. G. Sykes, D. Blume, and J. L. Bohn, Hyperspherical lowest-order constrained-variational approximation to resonant Bose-Einstein condensates, Phys. Rev. A **97**, 033608 (2018).
[22] T. K. Das and B. Chakrabarti, Potential harmonics expansion method for trapped interacting bosons: Inclusion of two-body correlation, Phys. Rev. A **70**, 063601 (2004).
[23] T. K. Das, S. Canuto, A. Kundu, and B. Chakrabarti, Behavior of a Bose-Einstein condensate containing a large number of atoms interacting through a finite-range interatomic interaction, Phys. Rev. A **75**, 042705 (2007).
[24] B. Chakrabarti and T. K. Das, Shape-independent approximation for Bose-Einstein condensates interacting through a van der Waals potential, Phys. Rev. A **78**, 063608 (2008).
[25] H. W. van der Hart, Collapse versus growth for a Bose-Einstein condensate with attractive interactions, Phys. Rev. A **62**, 013601 (2000).
[26] T. Sogo, D. V. Fedorov, and A. S. Jensen, Coherent atom–molecule oscillations with hyperspherical coordinates, J. Phys. B **38**, 2979 (2005).
[27] C.-N. Liu, T. Morishita, and S. Watanabe, Time-dependent hyperspherical studies for a two-dimensional attractive Bose-Einstein condensate, Phys. Rev. A **75**, 023604 (2007).
[28] H. Lee and C. H. Greene, Orbital variational adiabatic hyperspherical method applied to Bose-Einstein condensates, Phys. Rev. A **103**, 023325 (2021).
[29] S. T. Rittenhouse, M. J. Cavagnero, J. von Stecher, and C. H. Greene, Hyperspherical description of the degenerate fermi gas: s-wave interactions, Phys. Rev. A **74**, 053624 (2006).
[30] S. T. Rittenhouse and C. H. Greene, The degenerate Fermi gas with density-dependent interactions in the large-N limit under the K-harmonic approximation, J. Phys. B **41**, 205302 (2008).
[31] S. T. Rittenhouse, M. J. Cavagnero, and C. H. Greene, Collective coordinate description of anisotropically trapped degenerate Fermi gases, J. Phys. Chem. A **113**, 15016 (2009).
[32] D. Kushibe, M. Mutou, T. Morishita, S. Watanabe, and M. Matsuzawa, Aspects of hyperspherical adiabaticity in an atomic-gas Bose-Einstein condensate, Phys. Rev. A **70**, 063617 (2004).
[33] P. B. Blakie, D. Baillie, and S. Pal, Variational theory for the ground state and collective excitations of an elongated dipolar condensate, Commun. Theor. Phys. **72**, 085501 (2020).
[34] H. Hu and X.-J. Liu, Collective excitations of a spherical ultradilute quantum droplet, Phys. Rev. A **102**, 053303 (2020).
[35] K. Huang and C. N. Yang, Quantum-mechanical many-body problem with hard-sphere interaction, Phys. Rev. **105**, 767 (1957).
[36] T. D. Lee, K. Huang, and C. N. Yang, Eigenvalues and eigenfunctions of a Bose system of hard spheres and its low-temperature properties, Phys. Rev. **106**, 1135 (1957).
[37] Y. F. Smirnov and K. V. Shitikova, Method of K harmonics and the shell model, Sov. J. Part. Nuclei **8**, 344 (1977).
[38] J. Avery, W. Bian, J. Loeser, and F. Antonsen, Fourier transform approach to potential harmonics, Int. J. Quantum Chem. **63**, 5 (1997).
[39] F. Dalfovo, S. Giorgini, L. P. Pitaevskii, and S. Stringari, Theory of Bose-Einstein condensation in trapped gases, Rev. Mod. Phys. **71**, 463 (1999).
[40] I. S. Gradshteyn and I. M. Ryzhik, *Table of Integrals, Series, and Products* (Academic, New York, 1994).